Journal of Structural Geology 96 (2017) 54–64

Contents lists available at ScienceDirect

Journal of Structural Geology

journal homepage: www.elsevier.com/locate/jsg

# The fracture patterns of the Tin Tin anticline: Fracturing process during the foreland evolution in the Calchaquí Valley, northwestern Argentina

Mariano Hernández*, Juan R. Franzese

*Centro de Investigaciones Geológicas (UNLP-CONICET), diagonal 113 n° 275, B1904DPK, La Plata, Buenos Aires, Argentina*

ARTICLE INFO

*Article history:*
Received 17 October 2016
Received in revised form
19 January 2017
Accepted 26 January 2017
Available online 30 January 2017

*Keywords:*
Joints
Small-scale faults
Yacoraite formation
Foreland basement-cored fold
Eastern Cordillera
Northwestern Argentina

ABSTRACT

We present a field-based work which illustrates the fracture patterns of the carbonate-siliciclastic Yacoraite Formation in the Tin Tin anticline, a basement fault-related fold located in southern part of the Eastern Cordillera, northwestern Argentina. The fracture patterns include small-scale strike-slip faults (vertical shear fractures and *en echelon* arrays), thrust faults, extension fractures (joints, veins and normal faults) and stylolites. Extensional mesostructures were formed by along-foreland stretching, prior to the contractional ones that were formed by the layer-parallel shortening mechanism. Furthermore, all fractures are interpreted to be formed before or at the early stages of folding and thrusting during the Andean contraction, all of them belonging to the Eocene thrust belt-foreland system at the Calchaquí Valley of northwestern Argentina.

© 2017 Elsevier Ltd. All rights reserved.

## 1. Introduction

The study of small-scale structures (i.e. observable at outcrop scale, also known as mesofractures), and particularly those related to folds, has become increasingly important for the management of naturally fractured reservoirs of fold and thrust belts all around the world (Antonellini and Mollema, 2000; Hennings et al., 2000; Nelson, 2001). In northwestern Argentina, as well as along the Andes, much of the hydrocarbon is trapped in naturally fractured rocks, as is the Yacoraite Formation of the Cretaceous-Paleogene Salta Group (Mon and Salfity, 1995; Disalvo et al., 2002; Marquillas et al., 2005). This formation is a well-known carbonate fractured reservoir in the Subandean Ranges (e.g. Grosso et al., 2013) and it is exposed along the Eastern Cordillera (Fig. 1a). Despite its economic relevance, only few studies dealing with the fracture pattern of the Yacoraite carbonates have been published (e.g. Massaferro et al., 2003; Likerman et al., 2011; Grosso et al., 2013). More generally, studies linking mesoscale fractures and stress evolution in foreland thrust belts (e.g. Tavani et al., 2015) are not abundant in Argentina (e.g. Di Marco, 2005; Branellec et al., 2015).

In this work we illustrate the fracture patterns of the Yacoraite Formation in the Tin Tin anticline, a basement-cored fold located in the southern Eastern Cordillera of northwestern Argentina (Fig. 1a and b), representing an analogue for fractured reservoirs. Our aim is to contribute to the understanding of the structural setting during fracture formation and folding processes in naturally fractured reservoirs in northwestern Argentina.

## 2. Field area: Calchaquí Valley of NW Argentina

The Calchaquí Valley area is one of a series of N-S-oriented valleys that extends between the Puna and the Eastern Cordillera and further south into the Pampean ranges (Fig. 1a). Structurally, the area is characterized by broadly N-S-striking and west-vergent fault-related folds (such as the Tin Tin anticline) surrounded by large basement blocks (Fig. 1b). This structural framework is extensively assigned to the tectonic inversion of the Salta Group Basin resulted from Cenozoic Andean contraction (Grier et al., 1991; Mon and Salfity, 1995; Carrera et al., 2006; Carrera and Muñoz, 2008, 2013). The rift-related Salta Group Basin (Fig. 1d) developed during an extensional phase that took place during the Lower

* Corresponding author.
*E-mail addresses:* mhernandez@cig.museo.unlp.edu.ar (M. Hernández), franzese@cig.museo.unlp.edu.ar (J.R. Franzese).

http://dx.doi.org/10.1016/j.jsg.2017.01.011
0191-8141/© 2017 Elsevier Ltd. All rights reserved.

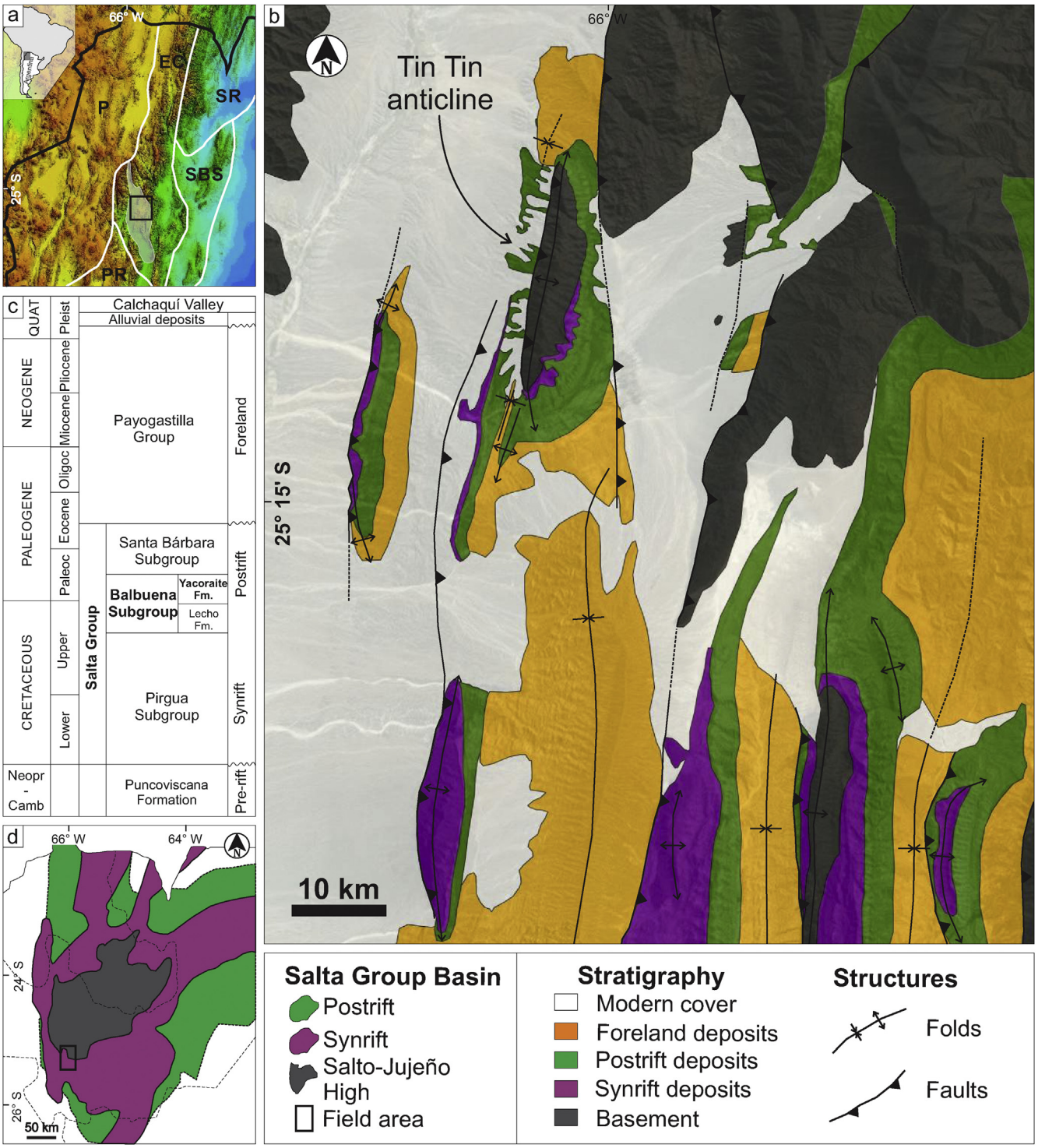


**Fig. 1.** a) Geological provinces of northwestern Argentina. P: Puna; EC: Eastern Cordillera; SR: Subandean Ranges; SBS; Santa Barbara System; PR; Pampean Ranges. Grey shade indicates the Calchaquí Valley. Black rectangle marks the study area showed in Fig. 1b. b) Geologic map of the study area showing the main structures and units. Dotted lines are inferred or unknown structures. c) Stratigraphic chart of the study area. d) Salta Group Basin deposit distribution. Black rectangle marks the Valle Calchaquí area showed in Fig. 1b.

Cretaceous and the Paleogene in NW Argentina. Isolated grabens characterized the early synrift stage. These sub-basins were placed around a structural basement high (Salto-Jujeño High) and were characterized by different orientations (Fig. 1d). The synrift deposits of the Pirgua Subgroup (Fig. 1c) were later overlaid by the early postrift deposits of the Balbuena Subgroup (Fig. 1c) when the decrease in tectonic subsidence and a relative sea-level rise allowed a shallow Atlantic marine ingression, in coincidence with humid conditions (Marquillas et al., 2005). The late postrift stage of the Salta Basin (Santa Bárbara Subgroup; Fig. 1c) is also characterized by thermal subsidence but different (drier) environmental conditions prevailed (Marquillas et al., 2005). Afterward, the onset of Andean contraction during the Paleogene led to the development of a foreland basin, filled by the Payogastilla Group in the Calchaquí

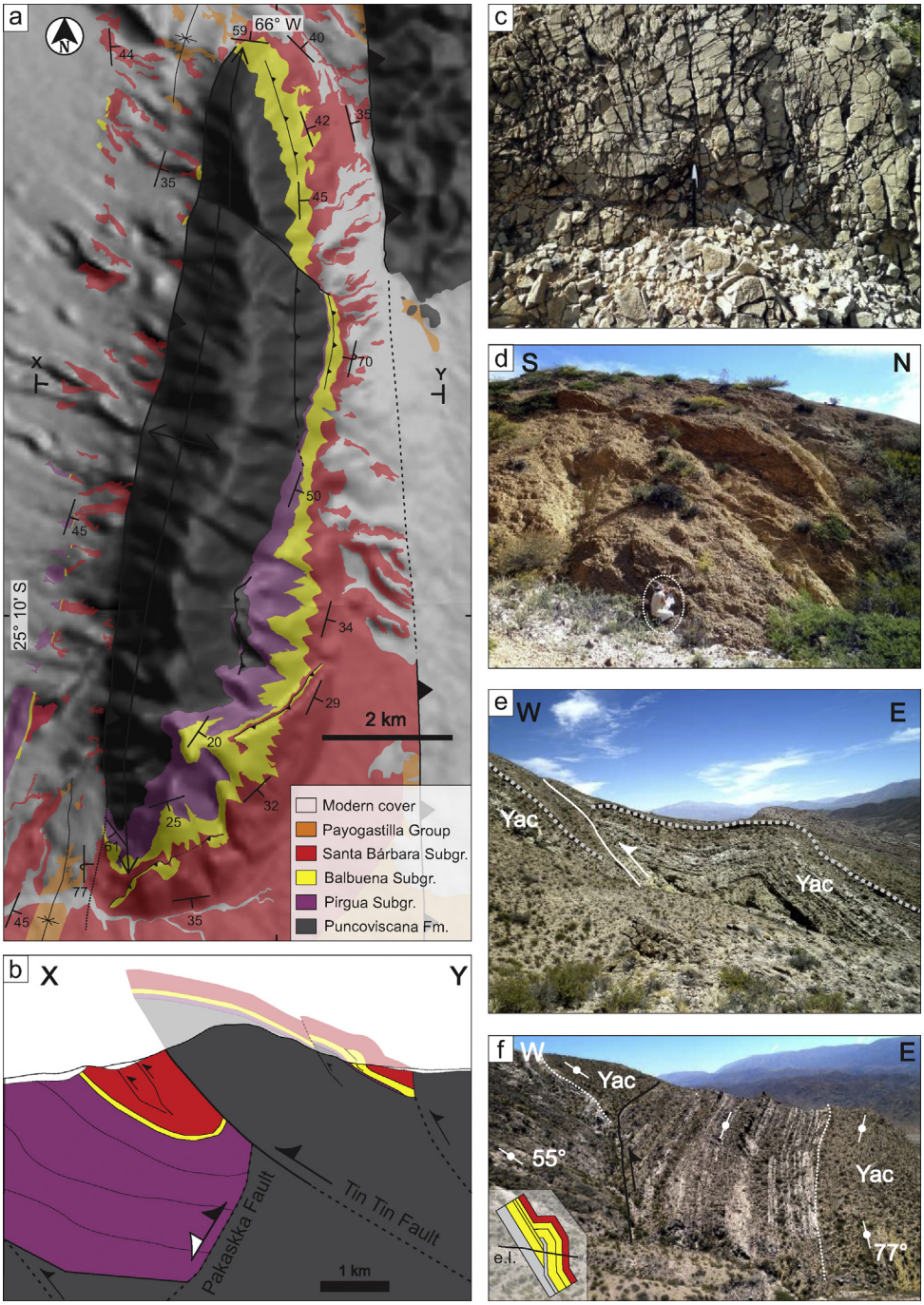


**Fig. 2.** a) Detailed geological map of the Tin Tin anticline. b) Schematic geologic profile of the Tin Tin anticline. X-Y trace is marked in Fig. 1a. The Pakkaska Fault and its western depocenter are based on Carrera and Muñoz (2013). c) Highly-strained bed of Yacoraite Fm. at the forelimb zone. d) Outcrop of Yacoraite Fm. at the forelimb zone. Diffuse bedding caused by high brittle strain. e) Fault-related folding in the backlimb of the anticline. f) Interpreted ramp-flat relationship at the backlimb (Hernández et al., 2016). Schematic diagram of the structure at the lower left corner (e.l.: erosion level). Yac.: Yacoraite Formation of Balbuena Subgroup.

Valley (Fig. 1b, d) with the subsequente tectonic inversion of the Salta Basin (Grier et al., 1991; Mon and Salfity, 1995; Carrera et al., 2006; Carrera and Muñoz, 2008, 2013).

Zonal cross-sections are poorly constrained in the study area because of the lack of seismic and well data. Carrera and Muñoz (2013) show an area-balanced cross-section located further south to the Tin Tin anticline, where the synrift deposits are exposed (Fig. 1b). Conversely, in the Tin Tin anticline there is little or no presence of Salta Group synrift deposits as the anticline belongs to the southwestern part of the Salto-Jujeño High (Mon and Salfity, 1995) where basement uplifts were dominant since Cretaceous times (Fig. 1b, d).

In detail, the Tin Tin anticline (Fig. 2a and b) is a NNE-SSW-striking, doubly-plunging, west-vergent basement-cored fold related to the Tin Tin east-dipping thrust (Hernández et al., 2016). Its sedimentary cover is exposed mostly in the backlimb and in the southern nose of the fold, whereas in the west limb of the Tin Tin anticline isolated and highly strained outcrops are exposed (Fig. 2c and d). This sedimentary cover was internally deformed (second-order scale folds and faults; Fig. 2e and f) little before and during

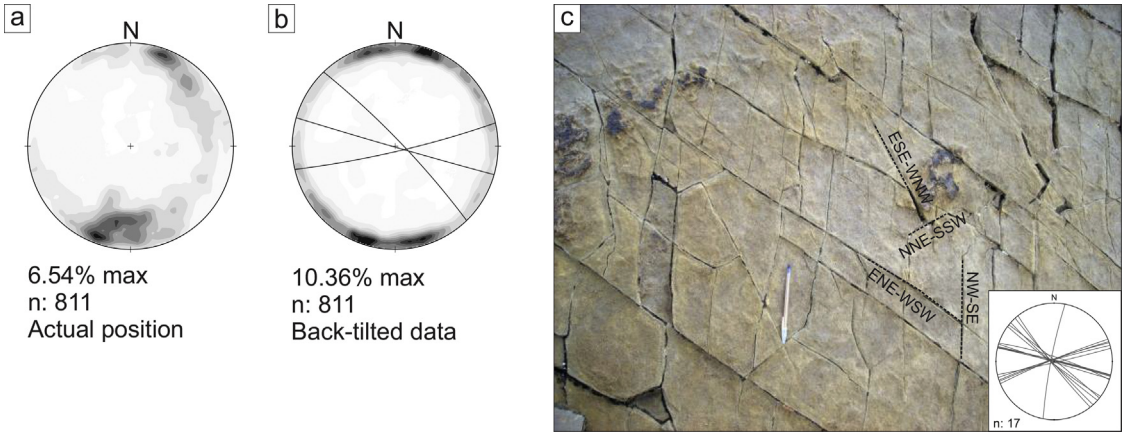


**Fig. 3.** Fractures plotted as contoured poles (1% area contours) to fractures on equal-area stereonets (lower hemisphere projections). Maximum percentage of contouring is indicated. a) Present orientation. b) After bedding dip removal (back-tilted or unfolded data considering each dip domain). Average fracture sets, determined from the pole concentrations, are plotted as great circles. c) Representative outcrop showing the common fracture sets, as show its equal-angle stereonet.

basement uplifting (Hernández et al., 2016).

The stratigraphic units exposed at the backlimb of the anticline, from base to top, are the Precambrian-Cambrian, low-grade metamorphic Puncoviscana Formation (basement core), the Cretaceous-Paleogene, rift-related Salta Group and the Cenozoic foreland Payogastilla Group (Grier and Dallmeyer, 1990; Grier et al., 1991; Salfity and Marquillas, 1994; Marquillas et al., 2005; del Papa et al., 2013).

Our study is mainly focused on the Yacoraite Formation, the early postrift sequence of the Salta Group (Marquillas et al., 2005), although the adjacent lower section of the overlying unit (Mealla Formation of Santa Barbara Subgroup, also postrift deposits) is locally included due to its similar mechanical behavior. The Yacoraite Formation is composed of alternating beds that range from few centimeters to up to 1.5 m thick. These beds are limestones, sandstones, stromatolitic boundstones (mainly in its upper section) and pelites that form a carbonate-silicoclastic mixed unit (Moreno, 1970; Marquillas et al., 2005). The whole Yacoraite Formation is 57 m thick at the Tin Tin anticline (Monaldi, 2001), although thrust faulting have thickened the unit up to 90 m at some parts of the backlimb (Hernández et al., 2016).

## 3. Data collection

Our field approach at the Tin Tin anticline was to measure small-scale fractures in many outcrops (measurement stations), grouping them into different sets based on type, abutting and orientation characteristics (e.g. Engelder and Peacock, 2001; Belayneh and Cosgrove, 2004; Fischer and Christensen, 2004; Tavani et al., 2011). Due to the geological characteristics of the anticline, most data come from its backlimb where scan lines were performed obtaining a dataset of more than 800 measures.

Shear fractures and *en echelon* fracture arrays were grouped and classified as faults (e.g. Tavani et al., 2011), and joints and veins as extension fractures (Engelder, 1987). Shear displacement along a fracture trace (on bed tops) is often very difficult to observe in the field (Stearns and Friedman, 1972; Davis and Reynolds, 1996; Mandl, 2005), so other complementary observations were taken into account in order to assess the origin of the observed fracture, such as the fracture orientation respect to bedding and respect to the fold axis, cross-cutting and angular relationship, fracture patterns and surface morphology (Bahat and Engelder, 1984; Engelder, 1987; Ameen, 1995). Thus, these observations and measurements as a whole were used to the ultimate fracture classification. In order to ease the proper interpretation of fracture data, fractures of each station were also back-tilted around a horizontal axis parallel to the local bedding strike (Tavani et al., 2006, 2011; Amrouch et al., 2010; Branellec et al., 2015).

## 4. Results: fracture types, orientation and distribution along the Tin Tin anticline

Fig. 3 show the whole fracture data collected in different dip domains along the Tin Tin anticline. As can be seen in the plots, most fractures are bed-perpendicular or are disposed at high angle respect to bedding. Although the measured strike of the fractures cover a wide range of directions, two high-frequency groups of fractures are evident in the contour plot, and those are the high-angle to bedding, ENE-WNW to E-W and ESE-WNW to SE-NW-striking fracture sets that commonly form a broadly oblique or ladder pattern (e.g. Fig. 3c).

### 4.1. Extension fractures: joints, veins and normal faults

Several outcrops exhibit centimeter-to-meters-long, bed-perpendicular and planar joints with plumose structure on their surface (Fig. 4a and b). These are by far the most common type of extension fracture and frequently exhibit a ladder or orthogonal pattern together with an orthogonal joint set (Fig. 4a, c). Where pavement surfaces are large enough, these fractures can be seen to extend up to tens of meters in trace length (Fig. 4a). The simplest outcrops commonly exhibit two main joint sets. The prominent one strikes from ENE-WSW to ESE-WNW (i.e. transverse to the fold axis), and are generally abutted by shorter, NNW-SSE- to NNE-SSW-striking (cross) joints, forming the above mentioned patterns. At some outcrops, the abutting relationships are ambiguous (Fig. 4c). These fractures are evenly distributed along the anticline without clusters in specific zones. Moreover, well-developed N-S-trending fractures are absent at the hinge zone (Fig. 4e), contrary to what would be expected in a folded layer (Price and Cosgrove, 1990). To a lesser extent, this group also contains ~ E-W-striking, high-angle to bedding fractures with normal displacement of centimeter to meters (Fig. 4d).

### 4.2. Shear fractures: small-scale strike-slip and thrust faults

Strike-slip faults are composed of bed-perpendicular, centimeters-to-meters-long, roughly planar fractures, sometimes with

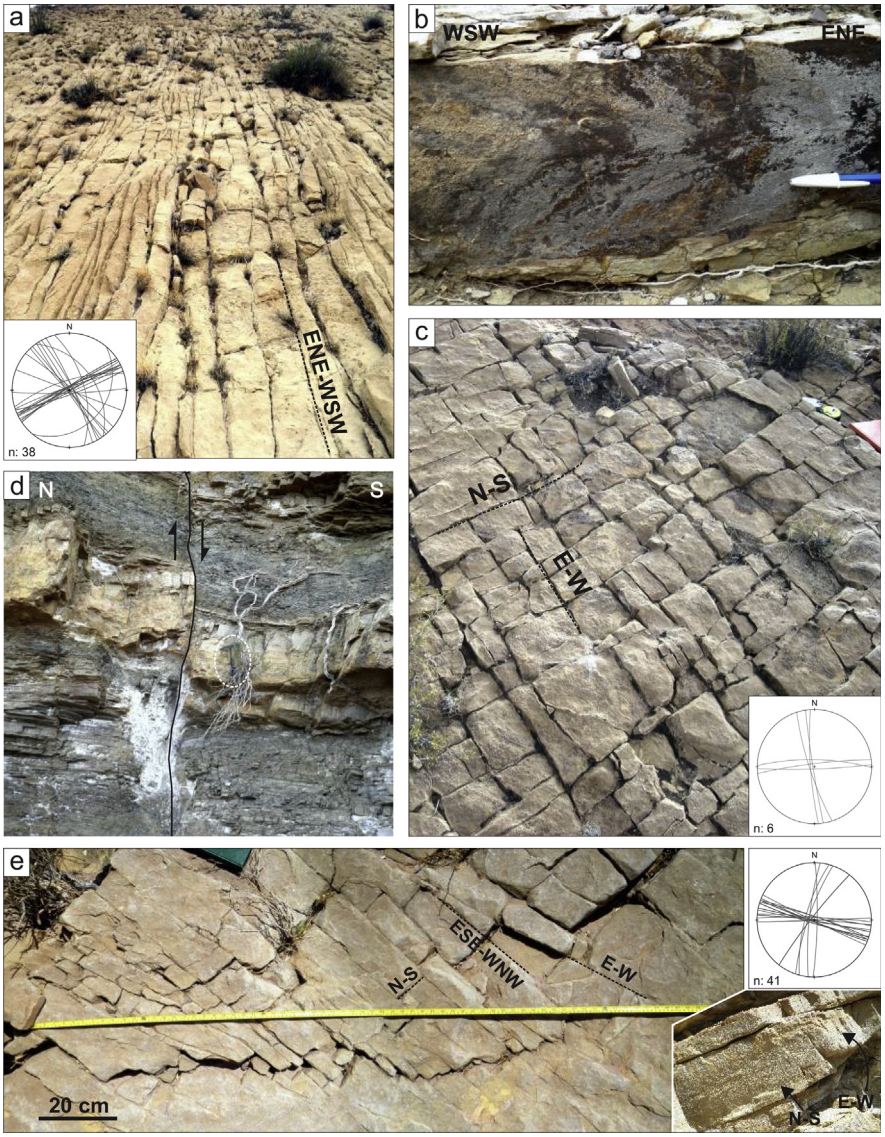


**Fig. 4.** Examples of extension fractures. a) ENE-WSW-striking, long-traced joints. b) Plumose structure belonging to the mentioned joint set. c) Orthogonal joint pattern with mutually cross-cutting relationship. d) ~E-W-striking, high-angle fracture with normal displacement. Downthrown block to the right (south). e) Outcrop located near of the fold hinge exhibiting the predominance of fold-perpendicular fractures and not well-developed hinge-parallel fractures. Lower right corner: Plumose structures (diffuse) on both ~ N-S and ~E-W joint sets.

dilatational jogs, and to a much lesser extent, of *en echelon* vein arrays (Fig. 5). Dextral strike-slip faults strike ENE-WSW to E-W, whereas sinistral strike-slip faults strike ESE-WNW to SE-NW. Even though the *en echelon* arrays are scarce, right-stepping (sinistral) *en echelon* vein arrays are more common and better developed than left-stepping (dextral) ones (e.g. Fig. 4b). Sinistral arrays are generally longer, wider and its individual component veins are more overlapped (e.g. Fig. 5b, c, d, e). Regarding to conjugate mesofractures, dihedral angles between faults are varied, as it can be seen in Fig. 3c (~60°), Fig. 5a–b (~30° and ~35°, respectively), Fig. 5d–e (~23° between the two faults), or in Fig. 5f (~39°).

Low-angle to bedding thrusts affect beds with different dips as well as meters-scale folds (Fig. 6b and c). The back-tilted (unfolded) stereographic plot shows a consistent NNE-SSW strike with both WNW- and ESE- dip-directions and dips of about 30°–40° (Fig. 6a). Some striated surfaces show a high pitch angle (~dip-slip movement), although the measurements are not sufficient enough for statistical analysis.

### 4.3. Other mesostructures: stylolites

Stylolitic seams are scattered along the backlimb of the Tin Tin anticline and they are associated to the high-carbonate content beds (i.e. limestones, grainstones). Few stylolitic surfaces were measured and they are disposed at high-angle respect to bedding. Most data come from their strike trace on the pavements, being sub-parallel to the fold trend (NNW-SSE to NNE-SSW strike; Fig. 6d). Thus, these measurements are taken into account as complementary data.

As has been described, the high-frequency transverse group of fractures (ENE-WSW- to ESE-WNW-striking sets) showed in Fig. 3b are composed of both strike-slip faults and extension fractures (joints, veins and few normal faults), whereas the fold-axis parallel group is composed of cross joint/veins, thrust faults and scarce stylolites. Something important to note is that at the southern fold nose, and specifically in the hinge zone and surroundings, small-scale faults show a clockwise deviation in strike from those at the


**Fig. 5.** Examples of small-scale strike-slip faults. a) Dextral and sinitral strike-slip faults, represented by shear fractures and *en echelon* vein arrays. Detailed sinistral en echelon array in lower right corner. b) Conjugate *en echelon* vein arrays. This example belongs to the same outcrop than picture 4a. c) ENE-WSW-striking, dextral strike-slip fault (fracture array). d) ENE-WSW-striking, dextral strike-slip fault (vein array). e) ESE-WNW-striking, sinistral *en echelon* vein array. Pictures from Fig. 4d and 4e belong to the same outcrop. f) Dextral and sinistral strike-slip faults, mainly represented by shear fractures and scarce *en echelon* vein arrays (top of the picture) and vein jogs (detailed at lower right corner).

backlimb, and therefore so are the inferred contraction direction (compare Fig. 7a with Fig. 6a for thrust faults and Fig. 5f (southern nose) with Fig. 5a (backlimb) for strike-slip faults). At some outcrops, cross-cutting relationship between sheared fractures and stylolitic seams indicates fracture reactivation with opposite kinematic (Fig. 7b and c). Moreover, outcrops exhibit varied fracture patterns, sometimes complex and difficult to interpret (Fig. 7d).

## 5. Data interpretation

Yacoraite Formation exposed at the limbs of the Tin Tin anticline holds a fracture pattern that includes joints and veins, shear fractures (small-scale faults) and stylolitic pressure solution seams.

The prominent sets of extension fractures (mostly joints) are predominantly oriented obliquely or at high angle to fold trend. The shorter cross-joints commonly abutting the main sets are hence oriented at low angle to the fold trend. Thus, ladder pattern is more common than orthogonal pattern. Few outcrops exhibit both orthogonal sets equally developed, thus indicating that these fractures are coevally formed, including those that form the ladder pattern (Bai et al., 2002). In term of strain, the predominance of the "transverse to fold trend" fractures (including the normal faults) is thus indicative of broadly N-S-directed stretching (Fig. 8, left).

Small-scale thrust faults are distributed all along the anticline, but they are better exposed at the northern sector of the anticline. The persistent low angle respect to bedding coupled with their occurrence in all structural positions indicate that these were formed before folding, during the layer-parallel shortening (LPS) stage that commonly predates thrusting (e.g. Tavarnelli, 1997; Branellec et al., 2015; Tavani et al., 2015). Striae data are not enough to make valid statistical analyses, but the few data are coherent with the E-W to ESE-WNW shortening direction inferred

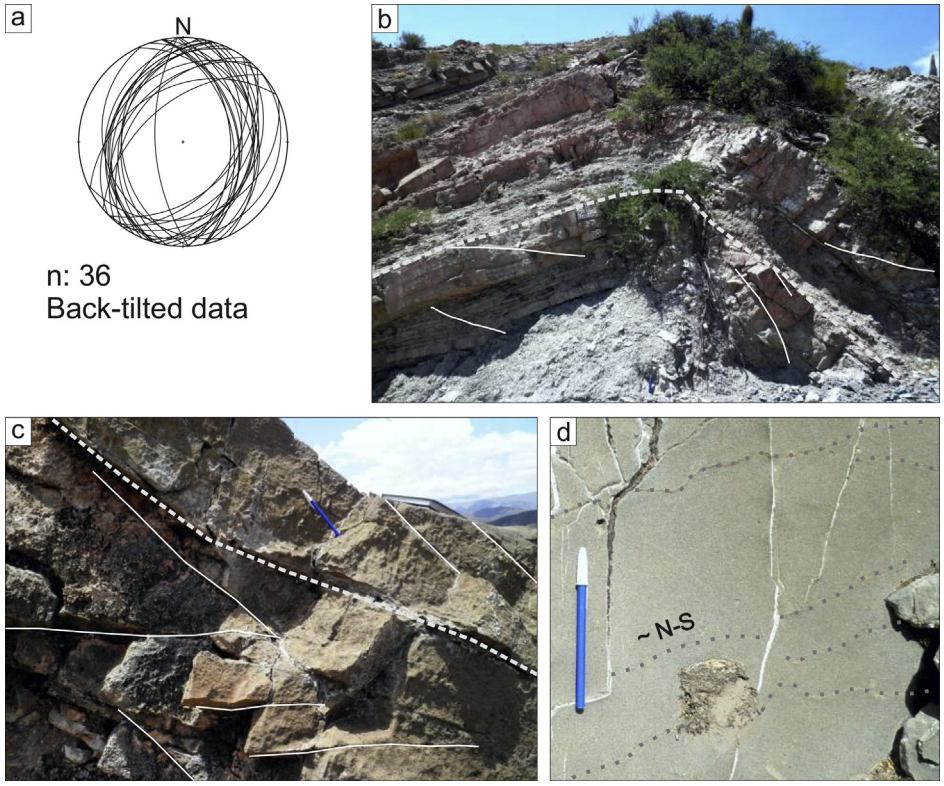


**Fig. 6.** a) Stereoplot of low-angle, small-scale thrust faults planes (equal-angle net, lower hemisphere projection). b) Low-angle fractures in folded bed. c) Close-up of low-angle fractures. d) Stylolite traces subparallel to the fold trend.

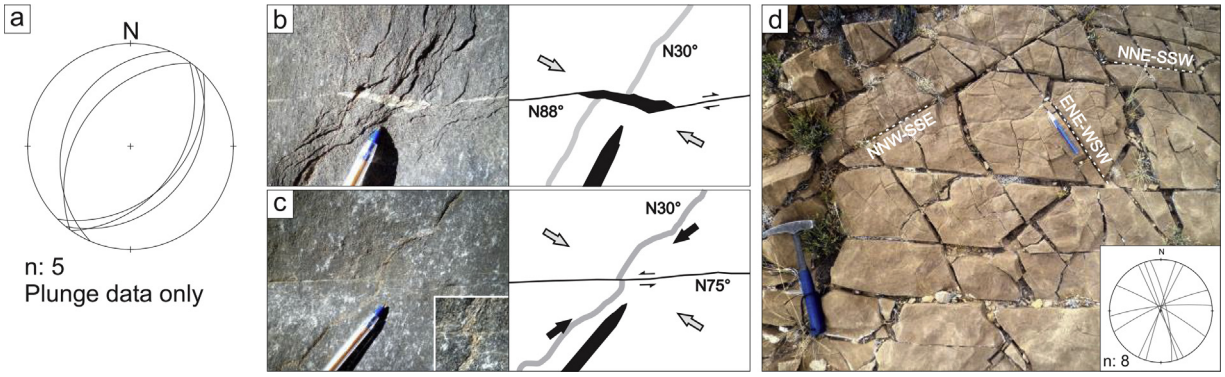


**Fig. 7.** a) Stereoplot of low-angle, small-scale thrust faults planes (equal-angle net, lower hemisphere projection). Data from the southern fold nose only. b) Stylolite displaced by shear fracture (trace azimuths after bedding dip removal). Both small-scale mesostructures (stylolite and shear fracture) could be interpreted as caused by the same local stress field. b) Same stylolite displaced by shear fracture with opposite kinematic, implying a change in local stress field. c) Multiple fracture pattern with unclear cross-cutting relationship.

for this zone (Daxberger and Riller, 2015).

Small-scale strike-slip faults exhibit a more or less consistent orientation through most part of the anticline. These could be grouped into small-scale, dextral and sinistral strike-slip faults, with ENE-WSW to E-W and ESE-WNW to SE-NW strike, respectively. Both small-scale thrust and strike-slip faults accommodate shortening parallel to bedding. The acute bisector of the small-scale strike-slip faults, which can be used to infer shortening directions, i.e. the approximated $\sigma_1$ orientation (Hancock, 1985; Price and Cosgrove, 1990; Smith, 1996; Belayneh and Cosgrove, 2010), indicates a broadly subhorizontal, E-W to ESE-WNW direction of contraction (Fig. 8, right), as it can be seen in Fig. 3b.

Cross-cutting relationships among all these mesostructures (the small-scale faults and the joints) are rather unclear. Although they were probably formed in different (and separate) moments as they belong to different stress states, these mesostructures are inferred to be formed prior or at the initial stages of folding, when beds were subhorizontal.

## 6. Discussion

### 6.1. Origin of fractures

Although no two outcrops share exactly the same fracture pattern, the fracture orientations are rather constant along the backlimb of the anticline. These fractures include extension joints and veins, small-scale strike-slip and thrust faults, and to a lesser extent, stylolites and normal faults. As we mention before, the

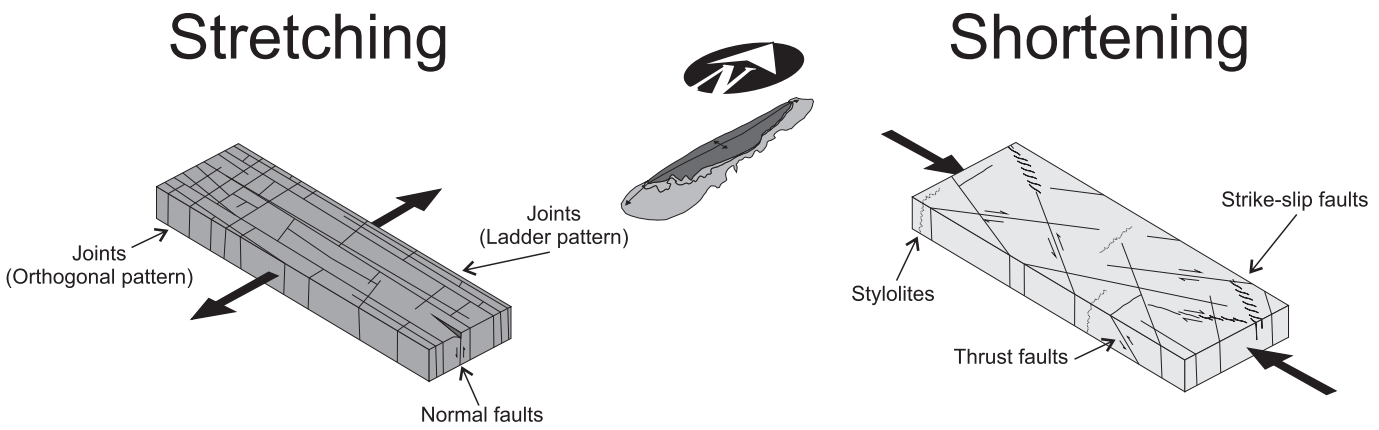


**Fig. 8.** Schematic diagrams of the fracture patterns in Tin Tin anticline. Left: transverse extension fractures formed by ~ N-S stretching. Right: Contractional mesostructures (small-scale faults and stylolites) formed by E-W to ESE-WNW shortening.

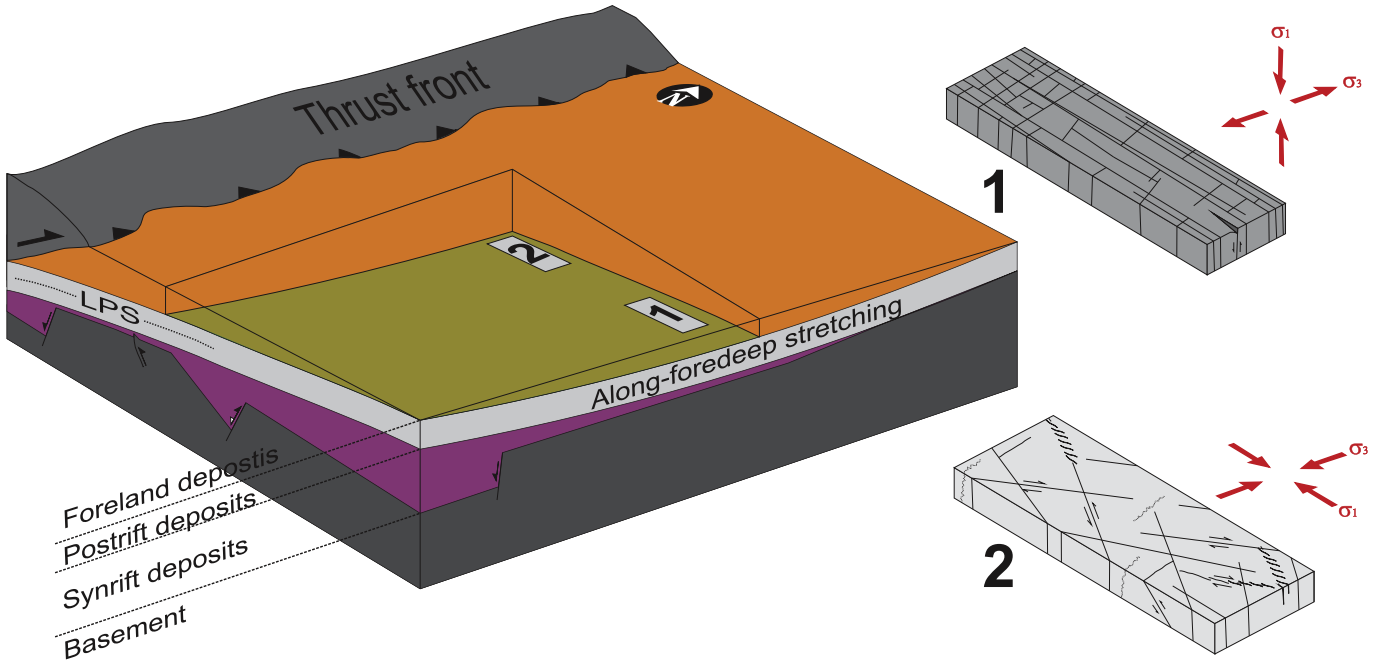


**Fig. 9.** Block diagram representing the Eocene thrust belt-foreland system and the occurrence of fractures. Extension fractures located in the belt-parallel stretched foredeep. Contractional mesostructures located near the thrust front, where layer-parallel shortening prevail. The orientation of the maximum and minimum principal stresses for each case is indicated.

strain interpretation of the mesostructures are different. So, varied mechanical processes could be invoked to explain the fracture patterns.

Both strike-slip and thrust faults are prone to be formed by a subhorizontal $\sigma_1$, with vertical $\sigma_2$ for the former and vertical $\sigma_3$ for the latter (strike-slip and thrust stress regimes respectively; Anderson, 1951). ~N-S-striking stylolites could be formed in both regimes, although the scarce data do not allow us to make any differentiation. These mesostructures are commonly associated to a layer-parallel shortening (LPS) mechanism (e.g. Geiser and Engelder, 1983), in which they accommodate shortening on sub-horizontal bedding, before the mayor thrusting and folding phase (Tavarnelli, 1997; Quintà and Tavani, 2012; Tavani et al., 2015).

The switch between $\sigma_2$ and $\sigma_3$ orientation is a phenomenon called the "$\sigma_2$ paradox" by Tavani et al. (2015). Although the causes of this phenomenon regarding to the Tin Tin anticline are unknown, our data correlates with the observations mentioned by Tavani et al. (2015) in which strike-slip faults are more abundant than thrust faults. Moreover, Beaudoin et al. (2016) indicate that strike-slip and thrust regimes alternate during LPS phase, but the former is the one that prevails. Nevertheless, the above mentioned mesostructures, as well as the Tin Tin anticline, are related to a widespread, sub-horizontal, E-W to ESE-WNW directed contraction (Fig. 8, right).

The other group of fractures is composed of the high angle to fold trend or "transverse" joints as well as the subparallel to fold trend (cross) joints, that are common features in folds (e.g. Stearns and Friedman, 1972; Price and Cosgrove, 1990). The origin of the bed-perpendicular transverse joints could be related to different mechanisms. One commonly invoked mechanism is the layer-parallel shortening (LPS) mechanism, in which these extension fractures would be in association with pressure solution cleavages and conjugated strike-slip faults, having the acute bisector striking parallel to the joints (Stearns and Friedman, 1972; Hancock, 1985; Tavani et al., 2006), and whose orientation responds to the

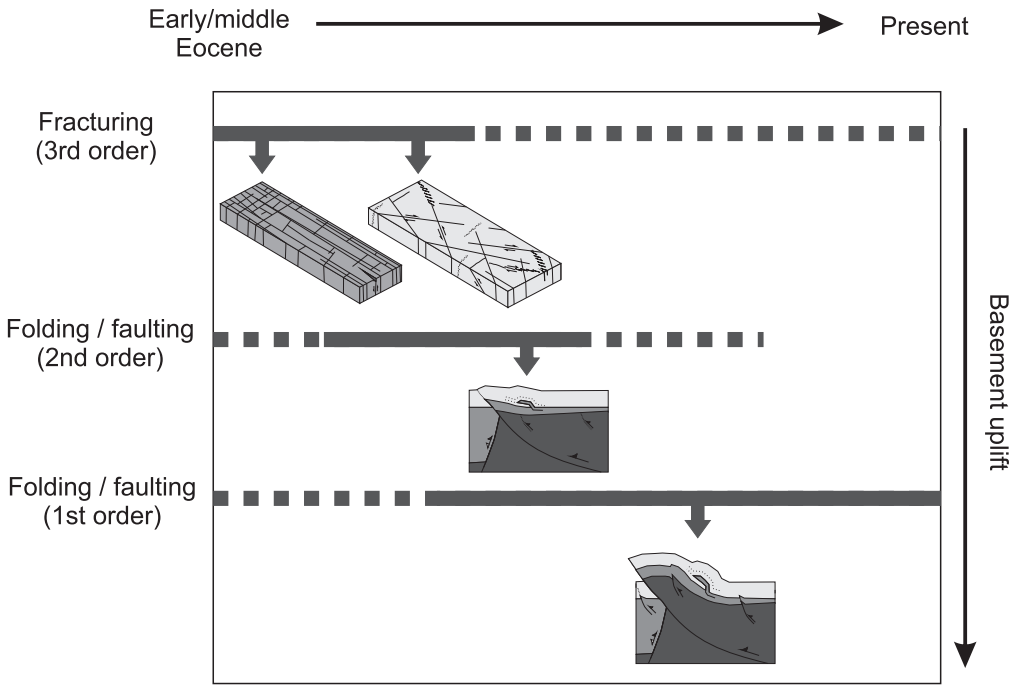


**Fig. 10.** Schematic (relative) structural evolution chart, representing the progression of the deformation from mesoscale fracturing to major thrusting and folding in the Tin Tin anticline area of the Calchaquí Valley.

regional compression direction ($\sigma_1$). In this scenario, extension fractures form parallel to a subhorizontal $\sigma_1$ and perpendicular to a subhorizontal $\sigma_3$ (strike-slip regime), assisted by an increase of fluid pressure during pressure solution cleavage development (e.g. Beaudoin et al., 2011; Quintà and Tavani, 2012), a common process in high-carbonate content units. Assuming that joints were formed by a subhorizontal $\sigma_1$, the occurrence of small-scale thrust faults would also be in association with bed-parallel joints and veins. Extension fractures with this orientation were not observed at the Tin Tin anticline. Moreover, the large number of joints compared to veins and the scarce occurrence of stylolites led us to infer that fluids did not play a key role in the formation of these transverse fractures. This inference, along with the lack of possible (but not frequent) bed-parallel extension fractures, allowed us to suggest that transverse joints were not formed by the LPS mechanisms.

Another mechanism to explain the transverse joints could be the effective belt-parallel (~N-S) extension. Transverse joints formed by broadly N-S extension could be originated by the along-strike stretching of the foredeep zone of a thrust belt-foreland basin system (Quintà and Tavani, 2012; Tavani et al., 2015 and references therein). The foredeep stretching results in the bending of the pre-foreland strata with an along-strike, upward-concave, curved profile (Tavani et al., 2015) and the formation of extensional structures to accommodate the strain (joints, veins, normal faults). This scenario requires a vertical maximum principal stress ($\sigma_1$) given by the sedimentary pile and a subhorizontal $\sigma_3$ parallel to the foredeep (Fig. 9). The early foreland deposits of the Calchaquí Valley and surrounding areas (Quebrada de Los Colorados Formation and equivalent units) were interpreted as foredeep deposits as well as wedge-top deposits (Hongn et al., 2011; Carrapa et al., 2012; del Papa et al., 2013) during Eocene times, although as is suggested by Carrapa et al. (2012) the along-strike palaeogeographical front of deformation might have been complex, with large eastward salients and reentrants. These complex geometries of the Eocene thrust front, possibly given by the reactivation of basement heterogeneities and previous rift-related normal faults (Hongn et al., 2007, 2010) could resulted in a heterogeneous, along-foredeep stretching. Thus, this mechanics could be invoked to explain the transverse joint sets that commonly strike ENE-WSW to E-W (i.e. NNW-SSE- to N-S-stretching), with the coevally formed cross-joints (Bai et al., 2002).

### 6.2. Fracture development and fracture-fold relationship

In the above section the interpretation of the origin of fractures driven by different mechanisms is stated. Joints and small-scale faults are then belonging to different episodes of fracturing during Eocene times, before the thrusting and folding phase. As is explained by Tavani et al. (2015), there is a progression in deformational stages in which the along-foredeep stretching is followed by the LPS stage when the thrust front approach (Fig. 9), with a change in $\sigma_1$ orientation from vertical to subhorizontal and perpendicular to the thrust front, before the onset of major thrusting and folding. Thus, we interpret an order in fracture formation in which jointing precedes the small-scale faulting. This implies that favourably oriented stretching-related joints (i.e. ENE-WSW to E-W-striking joints) may be sheared in the LPS phase (ESE-WNW shortening). Although evidence of joint surfaces containing both plumose ornament and striae is scarce, there is some signs to suspect the joint origin of some small-scale strike-slip faults, such as their large trace length despite their insignificant displacement and also the fact that these “faults” belongs to regularly spaced, bed-confined sets, both characteristics of joints (Wilkins et al., 2001). Moreover, it is suggested that re-activation of prefolding fractures, whatever their origin, may inhibit the development of classical folding-related deformation patterns (Tavani et al., 2015).

Summarizing, the described fracture patterns respond to different stress states (in space and time) but all fractures are associated to a foreland system during Eocene times, developed prior or at the early stages of folding and thrusting at the Calchaquí Valley area.

### 6.3. Progression of deformational stages at the Tin Tin anticline area

As well as the major part of NW Argentine, structuration of the Tin Tin anticline area has been determined by a widespread E-W to ESE-WNW contraction along the Cenozoic (Marrett et al., 1994; Mon and Salfity, 1995; Hongn et al., 2007; Carrera and Muñoz, 2008; Daxberger and Riller, 2015). In the beginning of Andean contraction during Eocene times, a N-S-trending thrust belt-foreland basin system was installed over a complex rift basin architecture (Grier et al., 1991; Mon and Salfity, 1995). Along the Calchaquí Valley area, a N-S-trending foredeep/wedge top depozone were located with the thrust front was westward (Decelles et al., 2011; Carrapa et al., 2012; del Papa et al., 2013). At this stage, transverse joints and their cross-joints and the scarce normal faults were formed by extension along the foredeep. Then, while the eastward-propagation thrust front approach, an E-W to ESE-WNW-oriented layer-parallel shortening phase prevailed at the Calchaquí Valley area, with the development of small-scale thrusts, conjugate strike-slip faults and scarce stylolites that accommodated shortening parallel to bedding. Here, the possible reactivation of previously formed bed-perpendicular joints could originate what in outcrop appear to be conjugate strike-slip faults with anomalous dihedral angles (Wilkins et al., 2001). Afterwards, the second-order and major (first-order, as the Tin Tin anticline) folding and thrusting phase took place with the consequently tectonic inversion of the area (Fig. 10). Thus, the fracture pattern of the Tin Tin anticline belongs to the initial stages of a progressive deformation that goes from meso- to macro-scale regarding the structural shortening of this area. It should be noted that, despite the inferred sequence of deformation, it is logical to assume that many more fractures were formed during the continuous process of exhumation until the Yacoraite Formation exposition.

## 7. Conclusions

The small-scale fractures of the Yacoraite Formation in the Tin Tin anticline are joints, veins, small-scale faults, and, to a lesser extent, stylolites and normal faults. These mesofractures are genetically related to a thrust belt-foreland basin system installed in the beginning of the Andean contraction during Eocene times in NW Argentina. Extension fractures are associated to a broadly N-S-directed stretching along the foredeep, whereas the small-scale faults and stylolites are associated to the subsequent ESE-WNW-directed layer-parallel shortening (LPS) phase. All fractures are interpreted to be formed prior or at the early stages of folding and faulting, which led to the tectonic inversion of the Calchaquí Valley area.

As naturally fractured reservoirs are often related to anticlines, this work reflect the importance of that not all fractures found on folds are a consequence of the folding process, and that the pre-folding fractures may play a very important role in fracture occurrence during the fold evolution, as changing or inhibiting the development of classical folding-related deformation patterns. This statement must be taken into account regarding the potential implications of the hydrocarbon exploration and production, focusing on the naturally fractured reservoirs of NW Argentina.

## Acknowledgments

The authors would like to thank the authorities and park guards of Los Cardones National Park for their kind help and support during the field work. This research was supported by CONICET (National Scientific and Technical Research Council of Argentina) and Pluspetrol S.A. Editor Joao Hippertt is gratefully thanked, as well as the reviewers Stefano Tavani and Fernando Hongn, whose meaningful comments and suggestions improved the early version of this manuscript.

## References

Ameen, M.S., 1995. Fractography: fracture topography as a tool in fracture mechanics and stress analysis. An introduction. In: Ameen, M.S. (Ed.), Fractography: Fracture Topography as a Tool in Fracture Mechanics and Stress Analysis, pp. 1–10. Geological Society Special Publication No. 92.

Amrouch, K., Lacombe, O., Bellahsen, N., Daniel, J.-M., Callot, J.-P., 2010. Stress and strain patterns, kinematics and deformation mechanisms in a basement-cored anticline: sheep Mountain Anticline, Wyoming. Tectonics 29, TC1005. http://dx.doi.org/10.1029/2009tc002525.

Anderson, E.M., 1951. The Dynamics of Faulting, second ed. Oliver and Boyd, Edinburgh.

Antonellini, M., Mollema, P.N., 2000. A natural analog for a fractured and faulted reservoir in dolomite: triassic sella group, northern Italy. AAPG Bull. 84, 314–344.

Bahat, D., Engelder, T., 1984. Surface morphology on cross-fold joints of the Appalachian Plateau, New York and Pennsylvania. Tectonophysics 104, 299–313.

Bai, T., Maerten, L., Gross, M.R., Aydin, A., 2002. Orthogonal cross joints: do they imply a regional stress rotation? J. Struct. Geol. 24, 77–88.

Beaudoin, N., Bellahsen, N., Lacombe, O., Emmanuel, L., 2011. Fracture-controlled paleohydrogeology in a basement-cored, fault-related fold: sheep Mountain Anticline, Wyoming, United States. Geochem. Geophys. Geosyst. 12 http://dx.doi.org/10.1029/2010GC003494 n/a-n/a.

Beaudoin, N., Koehn, D., Lacombe, O., Lecouty, A., Billi, A., Aharonov, E., Parlangeau, C., 2016. Fingerprinting stress: stylolite and calcite twinning paleopiezometry revealing the complexity of progressive stress patterns during folding—the case of the Monte Nero anticline in the Apennines, Italy. Tectonics 35, 1687–1712. http://dx.doi.org/10.1002/2016TC004128.

Belayneh, M., Cosgrove, J.W., 2004. Fracture-pattern variations around a major fold and their implications regarding fracture prediction using limited data: an example from the Bristol Channel Basin. In: Cosgrove, J.W.Y., Engelder, T. (Eds.), The Initiation, Propagation, and Arrest of Joints and Other Fractures. Geological Society, London, pp. 89–102. Special Publications 231.

Belayneh, M., Cosgrove, J.W., 2010. Hybrid veins from the southern margin of the bristol channel basin, UK. J. Struct. Geol. 32, 192–201.

Branellec, M., Callot, J.P., Nivière, B., Ringenbach, J.C., 2015. The fracture network, a proxy for mesoscale deformation: constraints on layer parallel shortening history from the Malargüe fold and thrust belt, Argentina. Tectonics 34, 623–647. http://dx.doi.org/10.1002/2014TC003738.

Carrapa, B., Bywater-Reyes, S., DeCelles, P.G., Mortimer, E., Gehrels, G.E., 2012. Late Eocene–Pliocene basin evolution in the Eastern Cordillera of northwestern Argentina (25°–26°S): regional implications for Andean orogenic wedge development. Basin Res. 24, 249–268. http://dx.doi.org/10.1111/j.1365-2117.2011.00519.x.

Carrera, N., Muñoz, J.A., Sàbat, F., Mon, R., Roca, E., 2006. The role of inversion tectonics in the structure of the Cordillera Oriental (NW Argentinean Andes). J. Struct. Geol. 28, 1921–1932.

Carrera, N., Muñoz, J.A., 2008. Thrusting evolution in the southern Cordillera oriental (northern argentine Andes): constraints from growth strata. Tectonophysics 459, 107–122.

Carrera, N., Muñoz, J.A., 2013. Thick-skinned tectonic style resulting from the inversion of previous structures in the southern Cordillera Oriental (NW Argentine Andes). In: Nemčok, M., Mora, A., Cosgrove, J.W. (Eds.), Thick-skin-dominated Orogens: from Initial Inversion to Full Accretion. Geological Society, London, pp. 77–100. Special Publications 377.

Davis, G.H., Reynolds, S.J., 1996. Structural Geology of Rocks and Regions, second ed. John Wiley and Sons, New York.

Daxberger, H., Riller, U., 2015. Kinematics of Neogene to Recent upper-crustal deformation in the southern Central Andes (23°–28°S) inferred from fault–-slip analysis: evidence for gravitational spreading of the Puna Plateau. Tectonophysics 642, 16–28.

DeCelles, P.G., Carrapa, B., Horton, B.K., Gehrels, G.E., 2011. Cenozoic foreland basin system in the central Andes of northwestern Argentina: implications for Andean geodynamics and modes of deformation. Tectonics 30, TC6013. http://dx.doi.org/10.1029/2011tc002948.

del Papa, C.E., Hongn, F.D., Powell, J., Payrola Bosio, P., Do Campo, M., Strecker, M.R., Petrinovic, I., Schmitt, A.K., Pereyra, R., 2013. Middle Eocene-Oligocene broken-foreland evolution in the Andean Calchaqui Valley, NW Argentina: insights from stratigraphic, structural and provenance studies. Basin Res. 25, 574–593.

Di Marco, L., 2005. Geología y fracturas en la estructura San Pedro, sierra del Alto Río Seco, Sierras Subandinas, provincia de Salta. Rev. de la Asoc. Geol. Argent. 60, 696–713.

Disalvo, A., Rodriguez Schelotto, M.L., Gomez Omil, R., Hoffman, C., Benitez, J., Hurtado, S., 2002. Los reservorios de la Formación Yacoraite. In: Schiuma, M., Hinterwimmer, G., Vergani, G. (Eds.), Rocas Reservorios de Las Cuencas Productivas de La Argentina, pp. 717–738, 5° Congreso de Exploración Y Desarrollo de Hidrocarburos.

Engelder, T., 1987. Joints and shear fractures in rock. In: Atkinson, B.K. (Ed.), Fracture Mechanics of Rocks. Academic Press, London, pp. 27–69.

Engelder, T., Peacock, D.C.P., 2001. Joint development normal to regional

compression during flexural-flow folding: the Lilstock buttress anticline, Somerset, England. J. Struct. Geol. 23, 259–277.
Fischer, M.P., Christensen, R.D., 2004. Insights into the growth of basement uplifts deduced from a study of fracture systems in the San Rafael monocline, east central Utah. Tectonics 23, TC1018. http://dx.doi.org/10.1029/2002tc001470.
Geiser, P., Engelder, T., 1983. The distribution of layer parallel shortening fabrics in the Appalachian foreland of New York and 'Pennsylvania: evidence for two non-coaxial phases of the Alleghanian orogeny. Geol. Soc. Am. Memoirs 158, 161–176. http://dx.doi.org/10.1130/MEM158-p161.
Grier, M.E., Dallmeyer, R.D., 1990. Age of the Payogastilla group: implications for foreland basin development, NW Argentina. J. S. Am. Earth Sci. 3, 269–278.
Grier, M.E., Salfity, J.A., Allmendinger, R.W., 1991. Andean reactivation of the Cretaceous Salta rift, northwestern Argentina. J. S. Am. Earth Sci. 4, 351–372.
Grosso, S., López, R., Vergani, G., O'leary, S., 2013. Reservorios carbonáticos naturalmente fracturados en el Yacimiento Caimancito (Formación Yacoraite), cuenca cretácica del noroeste Argentino. Rev. de la Asoc. Geol. Argent. 70, 53–69.
Hancock, P.L., 1985. Brittle microtectonics: principles and practice. J. Struct. Geol. 7, 437–457.
Hennings, P.H., Olson, J.E., Thompson, L.B., 2000. Combining outcrop data and three-dimensional structural models to characterize fractured reservoirs: an example from Wyoming. AAPG Bull. 84, 830–849.
Hernández, M., Franzese, J.R., Vergani, G.D., 2016. Caracterización estructural del anticlinal Tin Tin: aspectos sobre su estilo de deformación y su relación con la tectónica cenozoica del valle Calchaquí, provincia de Salta. Rev. de la Asoc. Geol. Argent. 73, 405–420.
Hongn, F., del Papa, C., Powell, J., Payrola Bosio, P., Petrinovic, I.A., Mon, R., 2011. Fragmented Paleogene foreland basin in the valles calchaquíes, NW of Argentina. In: Salfity, J.A., Marquillas, R.A. (Eds.), Cenozoic Geology of the Central Andes of Argentina. SCS Publisher, Salta, pp. 189–209.
Hongn, F., del Papa, C., Powell, J., Petrinovic, I., Mon, R., Deraco, V., 2007. Middle Eocene deformation and sedimentation in the Puna-Eastern Cordillera transition (23°-26°S): control by preexisting heterogeneities on the pattern of initial Andean shortening. Geology 35, 271–274.
Hongn, F., Mon, R., Petrinovic, I., Del Papa, C., Powell, J., 2010. Inversión y reactivación tectónicas cretácicocenozoicas en el Noroeste Argentino: influencia de las heterogeneidades del basamento neoproterozoico-paleozoico inferior. Rev. de la Asoc. Geol. Argent. 66, 38–53.
Likerman, J., Cristallini, E., Selles Martínez, J., 2011. Estudio de fracturas asociado al sistema de plegamiento en la localidad de tres cruces, provincia de Jujuy. In: 18° Congreso Geológico Argentino. Jujuy.
Mandl, G., 2005. Rock Joints. The Mechanical Genesis. Springer, Berlin/Heidelberg.
Marquillas, R.A., del Papa, C., Sabino, I.F., 2005. Sedimentary aspects and paleoenvironmental evolution of a rift basin: Salta Group (Cretaceous–Paleogene), northwestern Argentina. Int. J. Earth Sci. 94, 94–113.
Marrett, R.A., Allmendinger, R.W., Alonso, R.N., Drake, R.E., 1994. Late cenozoic tectonic evolution of the Puna plateau and adjacent foreland, northwestern argentine Andes. J. S. Am. Earth Sci. 7, 179–207.
Massaferro, J.L., Bulnes, M., Poblet, J., Casson, N., 2003. Kinematic evolution and fracture prediction of the Valle Morado structure inferred from 3-D seismic data, Salta province, northwest Argentina. AAPG Bull. 87, 1083–1104.
Mon, R., Salfity, J.A., 1995. Tectonic evolution of the Andes of northern Argentina. In: Tankard, A.J., Suarez Soruco, R., Welsin, H.J. (Eds.), Petroleum Basins of South America. AAPG Memoir, vol. 62, pp. 269–283.
Monaldi, C.R., 2001. Cratácico - paleógeno. In: Hongn, F.D., Seggiaro, R.E. (Eds.), Hoja Geológica 2566-III, Cachi. Provincias de Salta y Catamarca, vol. 248. Instituto de Geología y Recursos Minerales, Servicio Geológico Minero Argentino. Boletín, Buenos Aires, pp. 20–23.
Moreno, J.A., 1970. Estratigrafía y Paleogeografía del Cretácico Superior en la cuenca del Noroeste argentino, con especial mención de los Subgrupos Balbuena y Santa Bárbara. Rev. de la Asoc. Geol. Argent. 25, 9–44.
Nelson, R.A., 2001. Geologic Analysis of Naturally Fractured Reservoirs, second ed. Gulf Professional Publishing, Woburn.
Price, N.J., Cosgrove, J.W., 1990. Analysis of Geological Structures. Cambridge University Press, Cambridge.
Quintà, A., Tavani, S., 2012. The foreland deformation in the south-western Basque–Cantabrian Belt (Spain). Tectonophysics 576–577, 4–19.
Salfity, J.A., Marquillas, R.A., 1994. Tectonic and sedimentary evolution of the cretaceous-eocene Salta Group Basin, Argentina. In: Salfity, A. (Ed.), Cretaceous Tectonics of the Andes. Earth Evolution Sciences. Friedr. Vieweg and Sohn, pp. 266–315.
Smith, J.V., 1996. Geometry and kinematics of convergent conjugate vein array systems. J. Struct. Geol. 18, 1291–1300.
Stearns, D.W., Friedman, M., 1972. Reservoirs in fractured rock. In: King, R. (Ed.), Stratigraphic Oil and Gas Fields - Classification, Exploration Methods, and Case Histories, vol. 16. AAPG Memoir, pp. 82–106.
Tavani, S., Storti, F., Fernández, O., Muñoz, J.A., Salvini, F., 2006. 3-D deformation pattern analysis and evolution of the Añisclo anticline, southern Pyrenees. J. Struct. Geol. 28, 695–712.
Tavani, S., Mencos, J., Bausà, J., Muñoz, J.A., 2011. The fracture pattern of the Sant Corneli Bóixols oblique inversion anticline (Spanish Pyrenees). J. Struct. Geol. 33, 1662–1680.
Tavani, S., Storti, F., Lacombe, O., Corradetti, A., Muñoz, J.A., Mazzoli, S., 2015. A review of deformation pattern templates in foreland basin systems and fold-and-thrust belts: implications for the state of stress in the frontal regions of thrust wedges. Earth-Sci. Rev. 141, 82–104.
Tavarnelli, E., 1997. Structural evolution of a foreland fold-and-thrust belt: the Umbria-Marche Apennines, Italy. J. Struct. Geol. 19, 523–534.
Wilkins, S.J., Gross, M.R., Wacker, M., Eyal, Y., Engelder, T., 2001. Faulted joints: kinematics, displacement-length scaling relations and criteria for their identification. J. Struct. Geol. 23, 315–327.